

Full paper

Liquid-metal-elastomer foam for moldable multi-functional triboelectric energy harvesting and force sensing

Suryakanta Nayak^{a,*}, Yida Li^a, Willie Tay^c, Evgeny Zamburg^a, Devendra Singh^a, Chengkuo Lee^a, Soo Jin Adrian Koh^b, Patrick Chia^c, Aaron Voon-Yew Thean^{a,**}

^a Department of Electrical and Computer Engineering, National University of Singapore, 4 Engineering Drive 3, 117583, Singapore

^b Department of Mechanical Engineering, National University of Singapore, 9 Engineering Drive 1, 117575, Singapore

^c NUS School of Design & Environment, National University of Singapore, 4 Architecture Drive, 117566, Singapore

ARTICLE INFO

Keywords:

Energy harvesting
Porous TENGs
Nanocomposites
Liquid metal alloy
Force sensing
Wearable electronics

ABSTRACT

This article reports on a moldable soft porous composite of liquid metal alloy (LMA) and Ecoflex-0030 elastomer for the first time, where random pores in the composite behaves as tiny triboelectric nanogenerators (TENGs). The triboelectric foam produced a maximum peak-to-peak short-circuit current (I_{SC}) of ~ 466 nA (charge density = ~ 35 $\mu\text{C}/\text{m}^2$) and open circuit voltage (V_{OC}) of ~ 78 V for a sample of size $5\text{ cm} \times 5\text{ cm} \times 1\text{ cm}$, where the output current is $\sim 20\%$ higher than previously reported triboelectric foams based on PDMS and lead zirconate titanate (PZT)/carbon nanotube (CNT) of equivalent area. In addition, surface texture further increases the foam's softness and enhance the charge generation leading to a 36% increase in triboelectric charge (charge density = ~ 48 $\mu\text{C}/\text{m}^2$). A soft monolithic shoe insole is prepared, which produced a range of triboelectric responses in the order of μA in response to different modes of human motion. Upon jogging, the porous shoe insole with 3 wt parts of LMA in Ecoflex matrix, produce an instantaneous power of ~ 2.6 mW (instantaneous power density = 13 $\mu\text{W}/\text{cm}^2$). In addition, the insole also shows capacitive response to deformation, enabling the sensor to perform in-motion force and weight measurement.

1. Introduction

The soft electronics have attracted much attention for emerging applications in wearables, soft robotics, electronic skin, prosthetics, and implantable devices [1–10]. Especially for wearable electronics, soft moldable substrates can enhance the device conformability to human body shapes and offer better machine-body interface. This can enable new form-factor advantages over rigid electronics, especially for motion energy harvesting and sensing [11–14].

Generating static electrical charges by mechanical motion, triboelectric nanogenerators (TENGs) have gained much interests as energy harvesters for self-powered sensors for wearable electronics [15–30]. TENGs have been constructed with a wide variety of thin dielectric and conductor materials [15–19,31–34]. Many of these materials are flexible, soft, may be processed in low temperatures, and compatible with additive-based processing for flexible electronics [15–19,35]. As such, TENGs, as mechanical-to-electrical energy harvesters, can offer major large-area conformability advantage over typical piezoelectric harvesters with rigid crystals [35].

Wang's group have characterized well the basic modes of triboelectric generation: (i) vertical contact-separation, (ii) contact-sliding, (iii) single electrode, and (iv) free standing triboelectric-layer mode [36,37]. Mechanical, structural, and other material properties are all influential to charge generation and extraction [35,38,39]. Suitable optimized materials/composites and structures are necessary to harvest electrical energy/charges from human motion. Recently, it has been shown that triboelectric charge harvesting enhances upon increasing the softness of a material due to the improved contacts between different surfaces [40]. Although, TENG approaches based on conductor-elastomer composite material have been reported [41–46], the work largely focuses on thin-film structures rather than 3D volumetric form factors.

In this work, we investigate a soft moldable bulk structure that incorporates different triboelectrification, compounded through porous microstructures. We have used Galinstan [47] ($\text{Ga}_{62}\text{In}_{22}\text{Sn}_{16}$) LMA and Ecoflex to create a triboelectric foam where NaCl particles are used as a water-soluble sacrificial template to create pores in the elastomer. In all the composites, 10 g (parts) of Ecoflex is used as the base matrix. The

* Corresponding author.

** Corresponding author.

E-mail addresses: suryakanta.nayak@nus.edu.sg, suryakanta.iitkgp@gmail.com (S. Nayak), aaron.thean@nus.edu.sg (A.V.-Y. Thean).

concentration (by weight parts) of LMA and NaCl is varied with respect to the above base matrix (Ecoflex). The optimum composite with 3 wt parts of LMA in Ecoflex matrix (LMA:NaCl:Ecoflex = 3:5:10), produced a maximum peak-to-peak I_{SC} and V_{OC} . Further, by molding hexagonal-packed columnar surface textures, more contact-separation triboelectrification with respect to the electrodes was created. This increases the charge generation by 36%. For application point of view, in case of jogging, the porous composite with 3 wt parts of LMA (LMA:NaCl:Ecoflex = 3:5:10) in Ecoflex matrix (shoe insole), produce an instantaneous power of ~ 2.6 mW (instantaneous power density = $13 \mu\text{W}/\text{cm}^2$). The obtained instantaneous power density is ~ 18 and ~ 32 times higher than previously reported triboelectric foams based on PDMS and CNT/PZT respectively [41,42]. The above generated power can be useful to power certain wearable sensors [e.g. electrocardiogram (ECG) chip] [48]. On the application of a smart-sensor footwear (Fig. 1), we demonstrate a single-piece of shoe insole (area $\sim 200 \text{ cm}^2$). The insole produced a range of triboelectric responses, giving output currents in the order of μA in response to the stomping/jumping/jogging motion of a 73 kg person. In addition, the insole also shows capacitive response to deformation, enabling the sensor to perform in-motion force and weight measurement (Fig. 1). In existing triboelectric materials reported, the triboelectric signals are obtained dynamically. In our case, we show that apart from triboelectric signals, the capacitance of the composite can be utilized to measure both static as well as dynamic forces [49–51]. With sufficient thickness, our demonstrated shoe insole can operate in both contact-separation and compression mode. Moreover, it can be monolithically molded into any shape to conform well to the foot so that it can sense the forces and motion of the foot more intimately and accurately than piecewise sensors. The detailed working mechanism of the shoe generator/sensor is discussed in later sections.

2. Material synthesis and characterization

In this study, the foam is based on a porous liquid metal alloy-Ecoflex 0030 (LMA- Ecoflex) composite, prepared by sacrificial dissolution of NaCl particles (Sigma Aldrich, Singapore) from the composite matrix. The choice of LMA as the conductor allow us to control its uniform distribution in a volume by high-speed blending in the pre-cured elastomer. Due to its low melting temperature (-19°C), we preferred Gallium–Indium–Tin alloy (Galinstan) as the LMA.

The foam (Fig. 2a and b and Fig. S1 in supplementary information) has been prepared with varying concentration of LMA and NaCl particles in Ecoflex matrix and the formulations of different composites are given in Table S1 (supplementary information). The schematic presentation for the preparation of porous LMA-Ecoflex composites is given in Scheme S1 (supplementary information). We have used five samples for each measurement and their mean values are plotted.

The cavities present in the above porous composites can be seen clearly in both microscope (Fig. 2a, b and Fig. S2a) and scanning electron microscope (SEM) images [Fig. S3 (supplementary information)]. Residual undissolved NaCl crystals, are seen in the microscope image (Fig. 2a, b and Fig. S2a). Based on microscope inspection, the NaCl residues are typically less than 1–5% of the composite volume with respect to the pores, and we have found it to have negligible impact on the electrical and mechanical behavior of the foam. To quantify the effect of undissolved salt (1–5%) on the triboelectric output, two samples of dimension $1.5 \text{ cm} \times 1.5 \text{ cm} \times 1 \text{ cm}$ were cut from a previously prepared porous sample of dimension $5 \text{ cm} \times 5 \text{ cm} \times 1 \text{ cm}$. One of them was immersed in hot water for another 96 h to remove the residual (1–5%) salt. Finally, it was dried at 150°C for 48 h to remove all moisture, before the measurement. Then, output signal (I_{SC} and V_{OC}) was measured for both samples and found to be marginal at $\sim 33 \mu\text{C}/\text{m}^2$. Hence, it can be deduced that NaCl residue below 5% has negligible

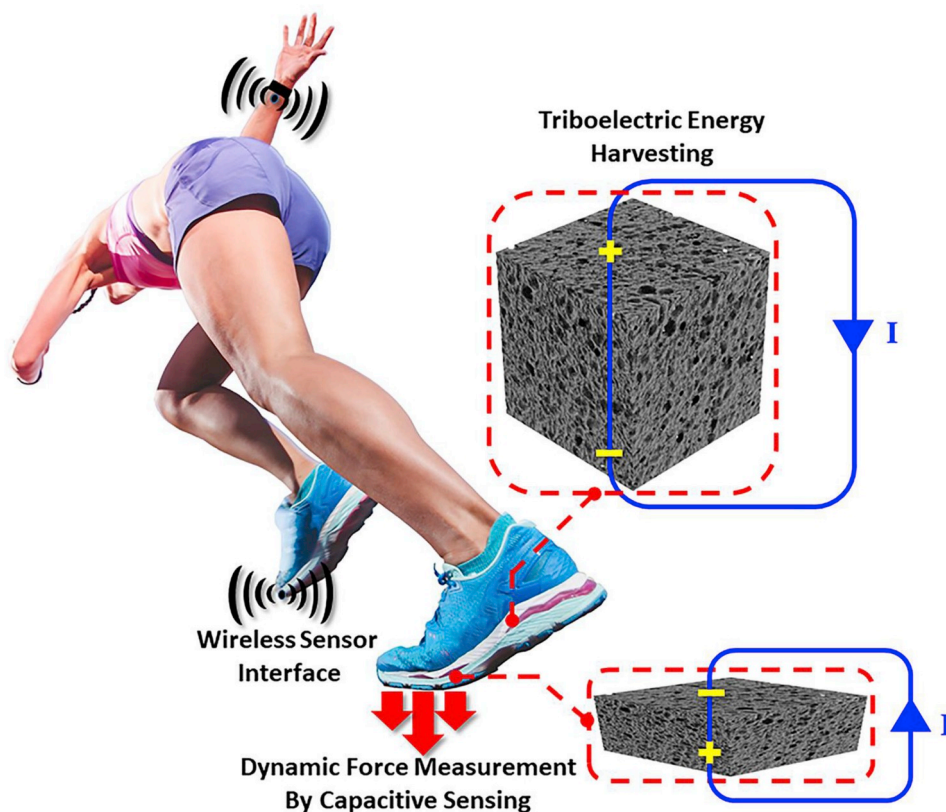


Fig. 1. Concept of smart footwear with energy harvesting, force sensing capabilities, and wireless data connectivity.

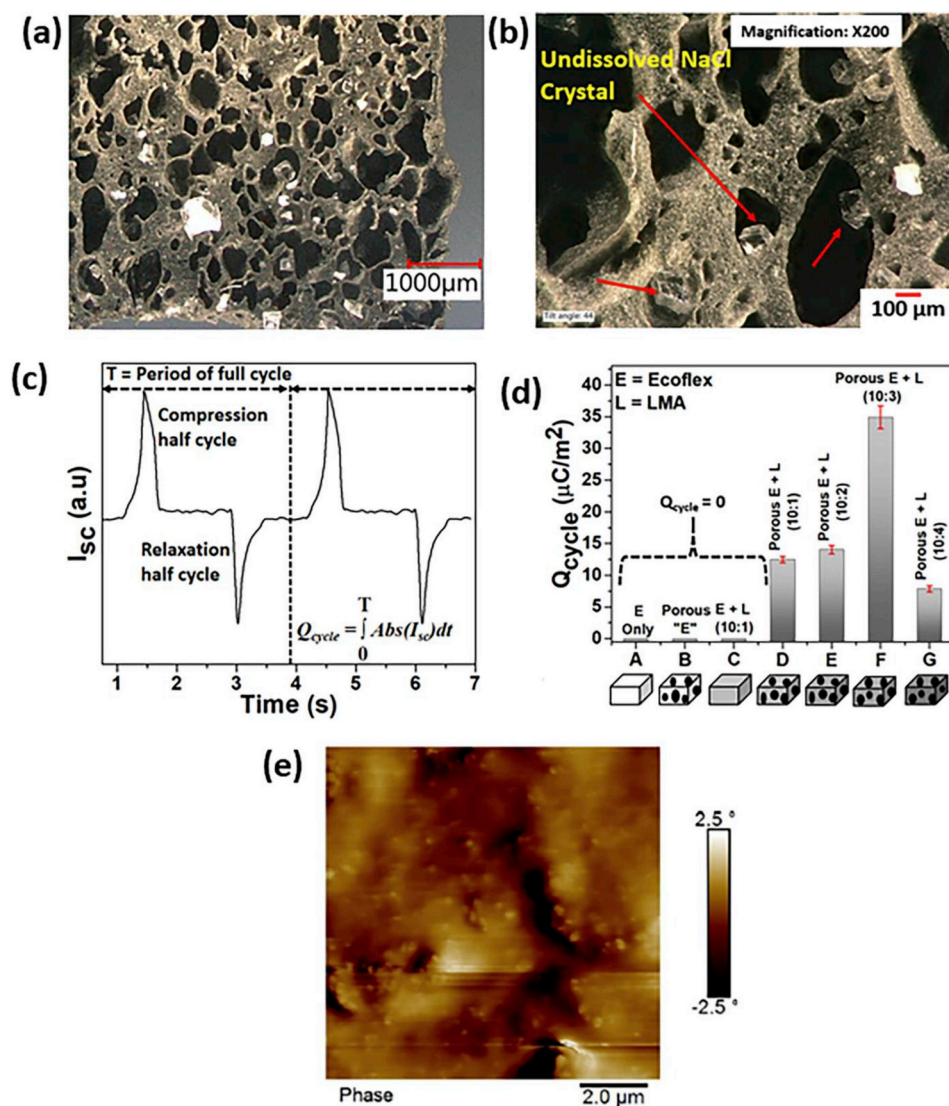


Fig. 2. (a) Low and (b) High magnification microscope images of porous nanocomposite containing 3 wt parts of LMA in Ecoflex matrix (LMA:NaCl:Ecoflex = 3:5:10). Some undissolved NaCl crystals remain (as indicated in figure b), (c) Short-circuit electrical current generated during the mechanical compression-and-relaxation cyclic deformation of the foam; charge density per cycle (Q_{cycle}) is the integral of the current over a single period of the mechanical cycle, normalized to the top surface area, (d) Triboelectric charge density for different samples of dimension 5 cm \times 5 cm \times 1 cm (compression depth = 5 mm) (A) pure Ecoflex (B) porous Ecoflex without LMA (NaCl:Ecoflex = 5:10), (C) non-porous composite with LMA (LMA:Ecoflex = 1:10), (D) porous composite with LMA (LMA:NaCl:Ecoflex = 1:5:10), (E) porous composite with LMA (LMA:NaCl:Ecoflex = 2:5:10), (F) porous composite with LMA (LMA:NaCl:Ecoflex = 3:5:10), and (G) porous composite with LMA (LMA:NaCl:Ecoflex = 4:5:10) [Maximum percent error \sim 6%], and (e) EFM image of LMA-Ecoflex composite (3 wt parts of LMA in Ecoflex) showing regions of different conductivity.

effect on the performance of the foam. The pore sizes are not uniform, and they are expected to follow the distribution of sacrificial NaCl crystals. The LMA appears to be well distributed between the pores and it is visibly dark compared to pure Ecoflex, due to the Gallium oxide formation [2]. The description of SEM images and mechanical properties of these composites have been provided in supplementary information.

3. Effects of foam composition and LMA loading

The pores and conductivity of the elastomer matrix play a crucial role for triboelectric properties of the foam. We sandwiched the foam between copper foil electrodes that are connected to a current source meter and a mechanical tester (Multitest 2.5-I, Mecmesin). The average charge density generated per cycle (Q_{cycle}) in response to mechanical deformation is measured by the time integral, over a full compression-relaxation cycle, of the absolute I_{sc} due to mechanical action (Fig. 2c). To test the bulk foam response instead of contact-surface effects, we ensured that the electrodes are well adhered to the foam under cyclic deformation to avoid any electrode-foam separation during testing.

Fig. 2d summarizes the experiment where we tested the elastomer in response to cyclic mechanical deformation, with respect to the presence of different concentration of LMA and pores. No charges were generated by the elastomer without the pores or LMA, confirming that both the

pores and the LMA are necessary for charge generation.

Increasing the LMA loading, up to 3 wt parts of LMA in Ecoflex matrix (LMA:NaCl:Ecoflex = 3:5:10), increases the charge generation, for the same pore density. For higher LMA concentrations, the charge output drops dramatically (Fig. 2d, Case F). The details on the electrical output have been provided in the supplementary information (Fig. S4). We found the charge degradation to be related to the excess conductivity and charge leakage resulting from LMA overload of the elastomer. This is discussed in the context of our single-cavity model, where we studied the pore electrostatics. In the meantime, we examine the foam's microstructure in terms of pore and LMA distribution.

Electrostatic force microscopy (EFM) scans were performed over a sample area of $10 \times 10 \mu m^2$ in the elastomer regions between the pores. We alternated the tip bias between 10 V and -10 V to detect the presence of surface charge. The regions of different contrast (dark/bright) in the EFM images indicate regions of different conductivities (Fig. 2e). Assuming that the high contrast regions represent large conductivity changes, the EFM scans suggest the LMA regions are not continuous between the pores, despite the visual uniformity of the inner-pore elastomer regions localized near the cavities. Therefore, we suspect the charges generated by the pores do not flow between the pores and they likely remain localized near the cavities. We assume that such mixed distribution of conductive and insulating regions continues into the inner surfaces of all the cavities. During mechanical compression of the

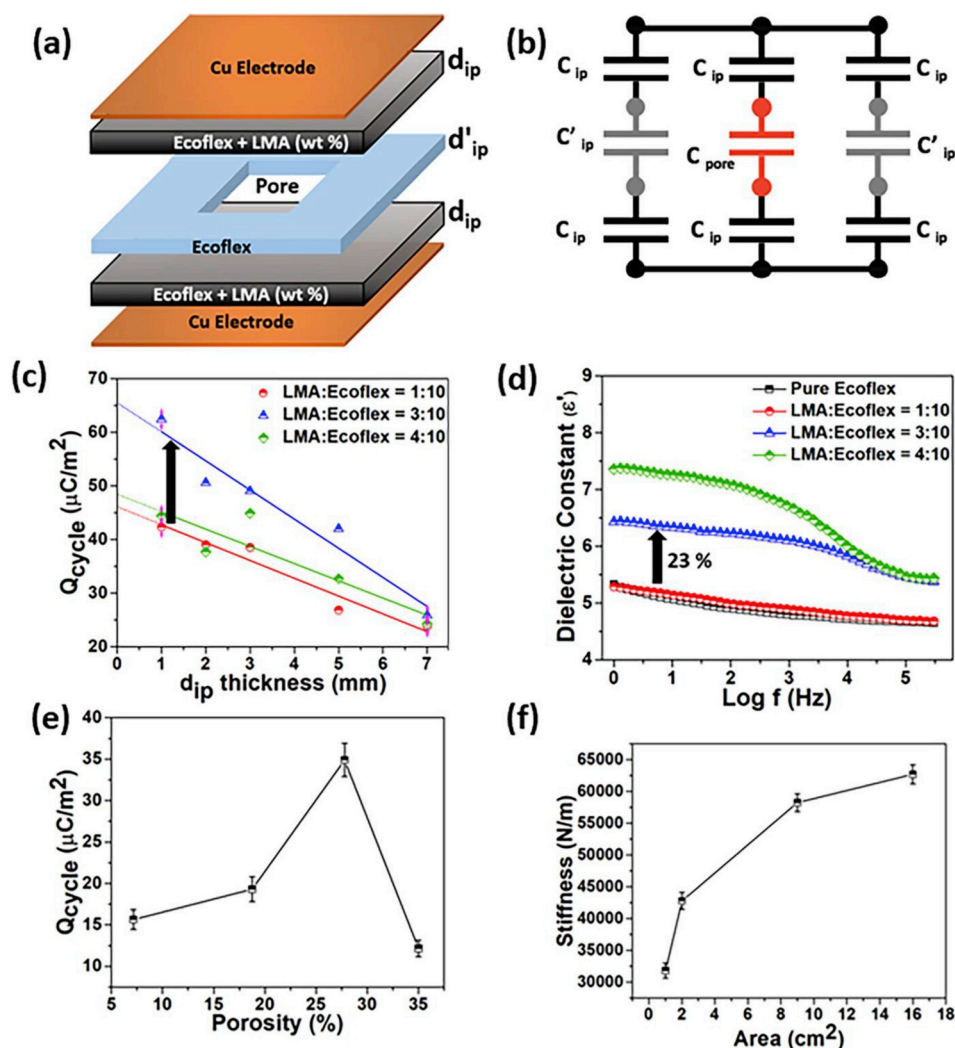


Fig. 3. (a) Schematic representation of the single cavity system where the middle layer is a pure Ecoflex elastomer with a cavity of dimension $3\text{ cm} \times 3\text{ cm} \times 0.5\text{ cm}$. Top and bottom layers (non-porous) are prepared with different LMA concentration (LMA:Ecoflex = 1:10, 3:10, and 4:10) and thicknesses (1 mm–7 mm), (b) A proposed equivalent passive circuit representation of the single pore structure (does not include triboelectrification and mechanical deformation), (c) Variation of output charge (per cycle) with sample thickness (1 mm–7 mm) for composites containing different concentrations of LMA [Maximum percent error $\sim 5\%$], (d) Frequency-dependent dielectric constant of LMA-Ecoflex composites with varying LMA concentrations, (e) Variation in output charge (Q_{cycle}) of composites containing 3 wt parts of LMA in Ecoflex matrix with different porosity. [Sample dimension = $5\text{ cm} \times 5\text{ cm} \times 1\text{ cm}$] [Maximum percent error $\sim 6\%$], and (f) Variation of stiffness with area of samples (LMA:NaCl:Ecoflex = 3:5:10) upon compressive cycles of depth 5 mm [Maximum percent error $\sim 4\%$].

foam (Fig. 2a and b), the inner surfaces of the cavities contact to produce electrification that is likened to contact-separation or contact-sliding triboelectrification effect.

We expect negative charges to be gained by the insulating Ecoflex regions due to its higher surface electronegativity as per triboelectric series and the positive charges build up in the conductive regions due to the LMA (Scheme S2) [41], when the inner surface of the cavities contact during compression. Upon force relaxation, the positive-negative charge separation produces an open-circuit potential difference (V_{OC}) that leads to a short-circuit current (I_{SC}). As the pore undergoes the relaxation, the I_{SC} reverses. Although we have shown that both the pores and LMA distribution are key to the triboelectric charge generation, the exact charge distribution in the complex random network of pores in the composite is difficult to describe and investigate. We expect the mechanism at the pore level to be analogous to the well-reported contact-separation mode (Scheme S3, Supplementary Information). As such, to understand how the fixed charge generation transfers to current under composite motion, we investigate it at the level of a single simplified model of a pore (Fig. 3a).

4. Single-cavity model for pore electrostatic study

To understand how LMA and the pores produce the triboelectrification, we constructed a large single-cavity test structure to simulate a single pore (Fig. 3a and b). Although mechanical properties of the

single-cavity structure may differ from the multi-pore foam, we expect it to provide qualitative trend on the electrical properties influenced by the material composition. The single cavity of dimension $3\text{ cm} \times 3\text{ cm} \times 0.5\text{ cm}$, is prepared from a pure Ecoflex elastomer sheet of thickness 0.5 cm, where it is used as the middle layer of the sandwiched structure (Fig. 3a). The single cavity is defined by three layers (d_{ip} layer sandwiched between two layers of d_{ip}), which simulate the inner-pore (ip) elastomer regions. The top and bottom layers (d_{ip}) connects the pore to the top and bottom copper (Cu) electrodes, while the side layers (d'_{ip}) separate the top and bottom d_{ip} layers. The equivalent passive circuit representation of the single pore structure is shown in Fig. 3b.

We vary the LMA concentration and thickness of the d_{ip} layers and characterize the triboelectric charge output (Fig. 3c and d). The inner-pore (ip) distance in the foam may be modeled by d_{ip} thickness. We found that as d_{ip} layer thickness decreases, the triboelectric charge output (Q_{cycle}) increases (Fig. 3c). In addition, we found that Q_{cycle} tend to increase with increasing LMA concentration from 1 to 3 wt parts in Ecoflex matrix (Fig. 3c). This Q_{cycle} difference between structures with different LMA concentrations reduces as d_{ip} increases. This is consistent with the elastomer composite's dielectric constant (ϵ_{ip}) increase with increased LMA incorporation. This would lead to enhancement of the equivalent capacitance per unit area between the pore and the Cu-electrodes ($C_{\text{ip}} \sim \epsilon_{\text{ip}}/d_{\text{ip}}$). Since $Q_{\text{cycle}} = C_{\text{effective}} \cdot V_{\text{OC}}$, increasing ϵ_{ip} enhances Q_{cycle} , and this enhancement is expected to diminish with increasing d_{ip} .

The change in dielectric properties has been separately characterized by dielectric spectroscopy (Navocontrol Alpha A spectrometer) for the same pore-free LMA-Ecoflex composites (Fig. 3d). Based on the frequency-dependent dielectric constant, increasing LMA concentration from 1 to 3 wt parts increased ϵ_{ip} by 23% (Fig. 3d). This confirms that LMA concentration increases the capacitive charge coupling between the pore and the electrodes. This is also consistent with EFM observation that the LMA is largely localized between the pores, leading to electric field coupling rather than charge transport between the pores.

However, beyond 3 wt parts LMA in Ecoflex matrix, we observe that Q_{cycle} decreases with increasing LMA concentration (Fig. 3d). Despite a further increase in ϵ_{ip} from 3 to 4 wt parts of LMA in Ecoflex matrix, as per dielectric spectroscopy (Fig. 3d), Q_{cycle} of composite with 4 wt parts of LMA in Ecoflex actually drops below that of the composite with 3 wt parts of LMA for all thicknesses. This is attributed to the charge leakage when LMA concentration becomes too high, and the elastomer capacitor can no longer hold the triboelectric charge upon generation (Fig. S5) [52–54]. In all porous composites, there may be some loss due to air breakdown as there are conductive LMA surrounding the micro-cavities. This suggests that for the triboelectric foam, it is important that the inner-pore elastomer should have high ϵ_{ip} , while remaining non-conductive, to enhance the capacitance for triboelectric charge due to

the pores. Based on the same capacitance argument, the capacitive charge coupling should also be enhanced by reducing the thickness of d_{ip} layer, or higher pore density in the random multi-pore foam structure.

5. Effects of foam porosity, mechanical stiffness, area, and thickness

The foam's pore density (porosity) can be modulated by increasing/decreasing the concentration of sacrificial NaCl particles. In Fig. 3e, we showed the output energy of samples (dimension = 5 cm × 5 cm × 1 cm) with a fixed 3 wt parts of LMA in Ecoflex matrix, where salt particle concentration was varied (LMA:NaCl:Ecoflex = 3:5/7/9:10) to get different porosity. We observed an increase in output charge with the increase in porosity. The maximum output charge was observed for the sample with ~28% porosity. However, we see a dramatic decrease in the output charge beyond this point. It appears that the excess of pores compromised the foam's structural stiffness; leading to significant pore collapse and the degradation of quick elastic recovery following mechanical compressions. This explains the degradation of the triboelectric charge generation.

We observe related dependence between the foam's mechanical

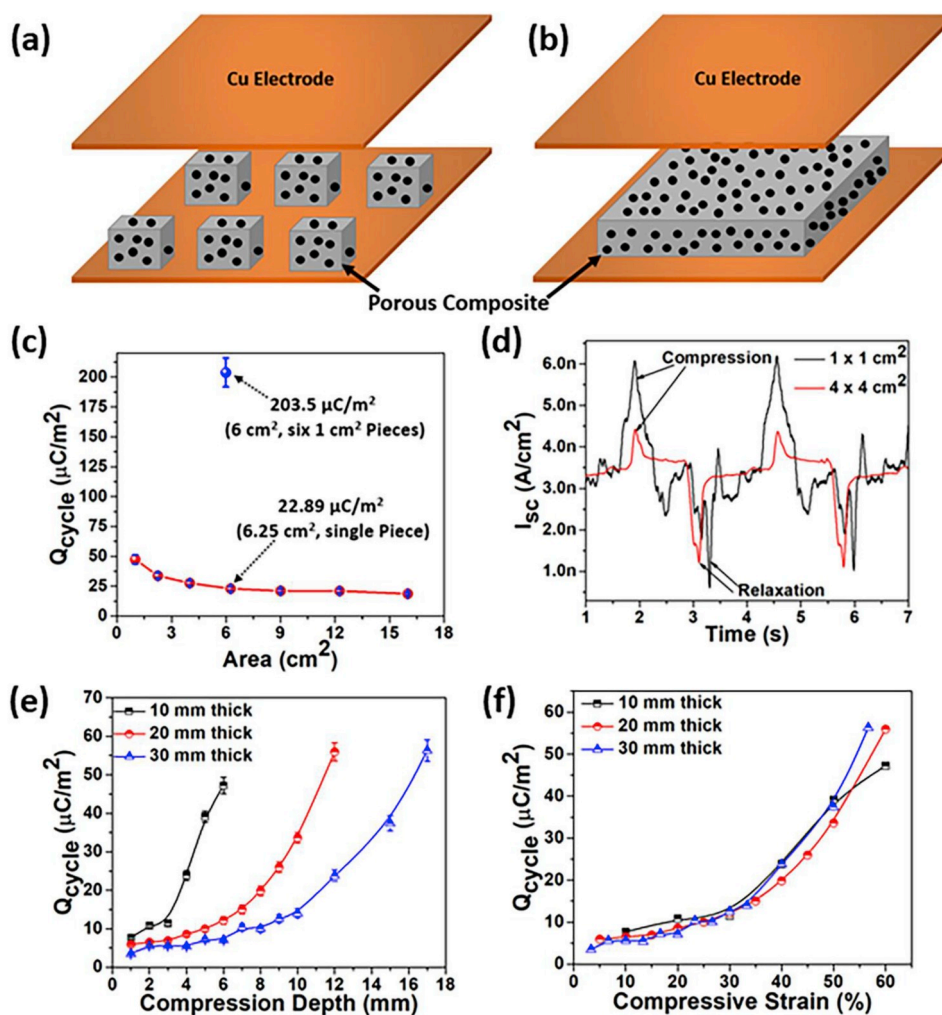


Fig. 4. (a) Schematic representation of testing conditions of 6-small pieces of small samples (1 cm × 1 cm), (b) one single piece (2.5 cm × 2.5 cm), (c) Variation of charge density with area of samples (LMA:NaCl:Ecoflex = 3:5:10) at a compression depth of 5 mm [Maximum percent error ~ 8%], (d) Comparison of current density for two different samples of area 1 cm × 1 cm and 4 cm × 4 cm, and (e and f) Variation of charge with compression depths and compressive strains for composite with 3 wt parts of LMA in Ecoflex matrix (LMA:NaCl:Ecoflex = 3:5:10) at three different thicknesses. [Maximum percent error ~ 8%].

properties and the triboelectric output in the form of area dependence. Fig. 3f shows the stiffness of square samples (thickness = 10 mm) with respect to different area upon compressive cycles of 5 mm depth. The stiffness of the composite materials was calculated from the maximum force upon 5 mm compression depth. The stiffness is defined as: $k = F/\delta x$, where k is the effective stiffness of the porous composite, F is the maximum force on the porous composite at 5 mm compression depth, and δx is the displacement produced by the force along the same degree of freedom. Here, the stiffness is determined by tracking the force (stress) needed to produce the same compression depth (strain). Due to the increased contribution of the edges, the samples become softer (lower stress/strain) when the area decreases (e.g. 31750 N/m for $1 \times 1 \text{ cm}^2$ as compared to 62765 N/m for $4 \times 4 \text{ cm}^2$) (Fig. 3f). Fig. 4a and b shows the schematics for the test condition of 6-small pieces ($1 \text{ cm} \times 1 \text{ cm}$) of samples and one single piece ($2.5 \text{ cm} \times 2.5 \text{ cm}$) respectively. There is an area dependence in the Q_{cycle} ; with a significant increase for samples below 4 cm^2 (Fig. 4c).

Close inspection of the I_{SC} response to cyclic deformation reveals correspondingly different features for the small $1 \times 1 \text{ cm}^2$ (softer) versus the larger $4 \times 4 \text{ cm}^2$ (stiffer) sample (Fig. 4d). Being softer, smaller samples show broader I_{SC} peak response during the compression cycle, leading to higher charge generation (area under I_{SC} curve) due to compression. In contrast, the larger sample, being stiffer, produce lower triboelectric charge under compression (and relaxation). In addition, secondary I_{SC} peaks (Fig. 4d) appear to become more prevalent in the smaller samples; due to increased sensitivity to non-uniform mechanical relaxation of the randomly-distributed pores, as the foam becomes softer. Given that samples of smaller area (Fig. 4a) produce a larger charge density as compared to a single-piece with a larger area (Fig. 4b). It would be intuitive to utilize distributed smaller samples to form a larger area to enhance the triboelectric output. Indeed, when 6 pieces of sample of size $1 \text{ cm} \times 1 \text{ cm}$ each are connected in parallel (total area = 6 cm^2), the resultant output is $203.5 \mu\text{C}/\text{m}^2$, which is more than a single larger piece of sample (6.25 cm^2 ; $22.89 \mu\text{C}/\text{m}^2$, Fig. 4c).

We have characterized the thickness dependence of the foam by cyclic deformation of $5 \text{ cm} \times 5 \text{ cm}$ square samples of three different thicknesses (10, 20, and 30 mm). We studied the effect of compression up to 60% compressive strain and observed that there is continuous increase in the output charge, when the compression depth increases for samples of all thicknesses (Fig. 4e). By varying the compression depths, it is seen that higher Q_{cycle} is produced for thinner samples, compared to thicker ones, for a given compression depth. However, when the output charge is normalized by fractional compressive depth with respect to the sample thickness (Strain = compression depth/sample thickness), Q_{cycle} follows identical dependence (Fig. 4f). Hence, Q_{cycle} is only dependent on percent volume change of the foam, confirming that the foam behaves as a volumetric triboelectric generator.

6. Monolithic foam molding to enhance triboelectric generation

In addition to electrification due to the compression-relaxation deformation of the foam; the contact and separation of the top copper electrode with respect of the composite foam (Scheme S3, supplementary information) can also be applied to generate further charges by mechanical motion (Fig. 5). For a $5 \text{ cm} \times 5 \text{ cm} \times 1 \text{ cm}$ flat foam with 3 wt parts LMA in Ecoflex matrix (LMA:NaCl:Ecoflex = 3:5:10), we found the peak-to-peak output current of 212 nA (Fig. 6a) and voltage of 28 V (Fig. 6b) upon contact-separation triboelectrification. However, we need soft spring-like structural behavior to support the electrode-to-foam separation that can be modulated by compression-relaxation motion, to exploit this additional mode of electrification.

To this end, we molded a series of hexagonally-packed soft round columns surface support structures for the ‘‘Cu’’ electrode (Figs. 5b and 6c). The surface support structures not only increased the contact surface area, they effectively segmented a significant volume of the foam. This reduces the effective foam stiffness, which is expected to further enhance the energy harvesting of compressive motion, as previously discussed. After optimizing the LMA loading and porosity for mechanical and electrical output, we characterize the performance of a

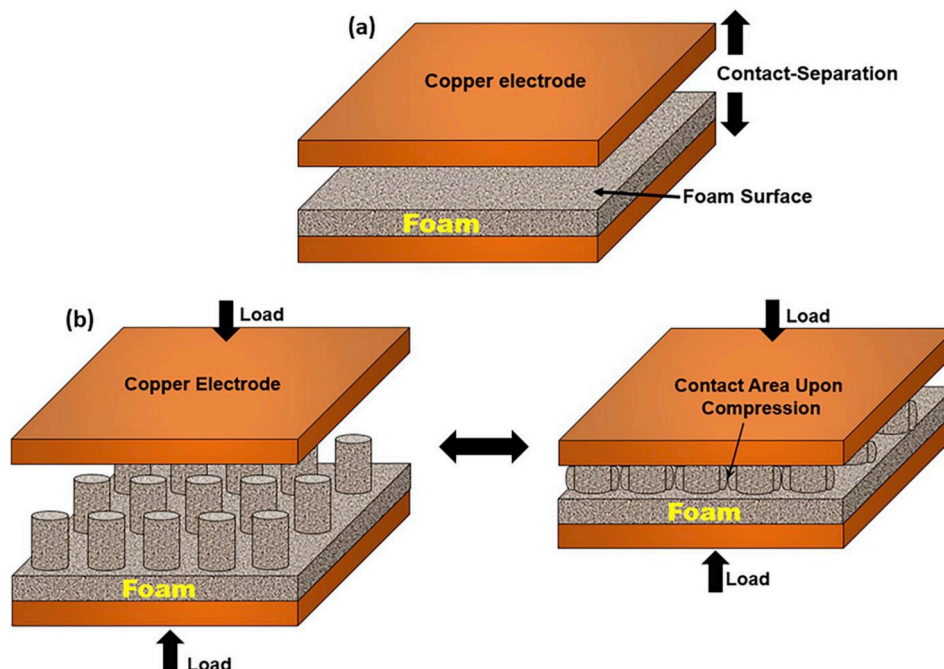


Fig. 5. Schematic representation of (a) contact-separation between top electrode and porous LMA-Ecoflex composite and (b) compression modes of sample with hexagonally packed columnar surface textures.

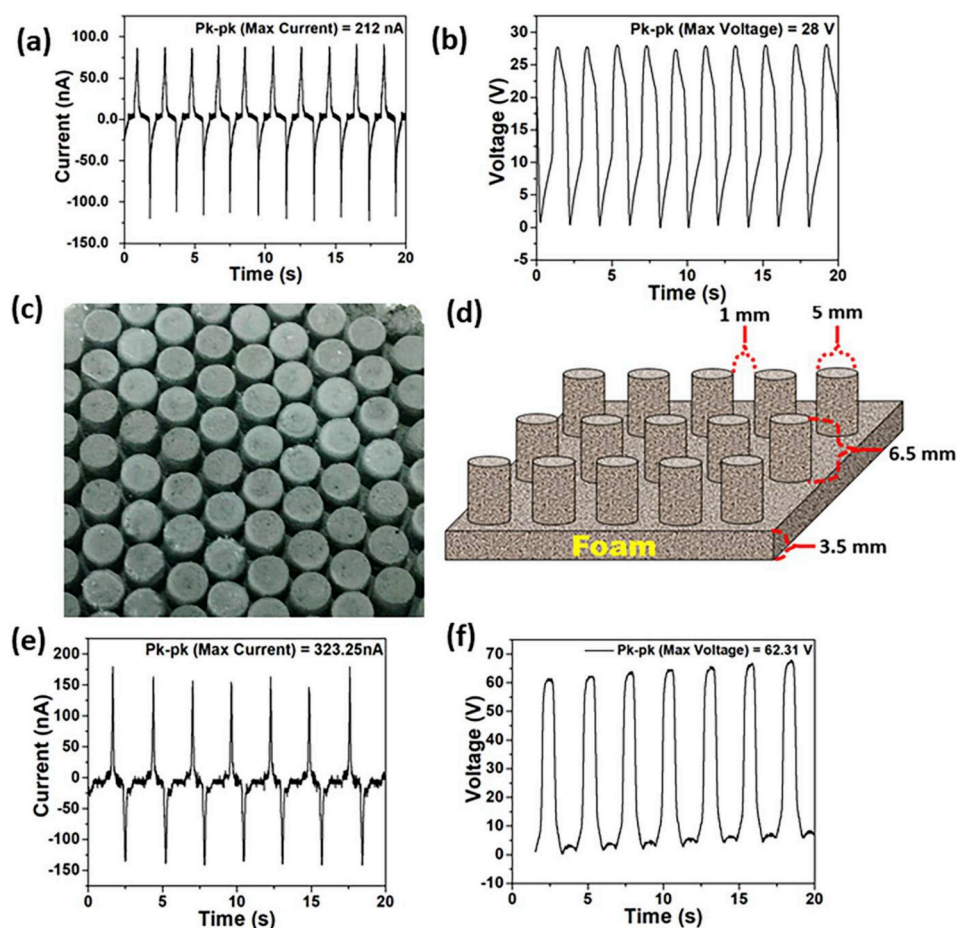


Fig. 6. Peak-peak (a, b) current (max ~ 212 nA) and voltage (max ~ 28 V) of flat porous LMA-Ecoflex composite (LMA:NaCl:Ecoflex = 3:5:10) measured at an operation frequency of ~ 0.4 Hz, (c) Photograph of a piece of porous pimple structured sample, (d) schematics of the cross-sectional image of the porous pimple structured sample; peak-peak (e) current (I_{SC}), and (f) voltage (V_{OC}) for pimple structured porous LMA-Ecoflex composites with 3 wt parts of LMA in Ecoflex matrix (LMA:NaCl:Ecoflex = 3:5:10) under 5 mm compressive cycles and at an operation frequency of ~ 0.4 Hz [active sample area = 12.56 cm 2].

5 cm \times 5 cm \times 1 cm sample. In this structure, thickness of the base composite and the columns are 3.5 mm and 6.5 mm respectively (Fig. 6d).

Under mechanical compression-relaxation cyclic testing (Fig. 5b), we measured an I_{SC} and V_{OC} of ~ 324 nA (charge density = ~ 48 $\mu\text{C}/\text{m}^2$) and ~ 63 V respectively (Fig. 6e and f). By increasing the effective surface of the elastomer, we show that higher triboelectric charge density for the foam can be achieved. There is some effect of contact-separation between different columns and also with the copper electrode (upon compressive cycles) on the overall output charge/energy (Fig. 5b). We used the above 3D-pimple structured model to prepare a full shoe insole (Fig. 7a) and studied its output current (I_{SC}) and voltage (V_{OC}) with respect to different modes of human motion, which is discussed in later section. To check the stability of LMA-Ecoflex TENG, we have carried out more than 10,000 cycles of pressing and releasing (at compression depth = 5 mm) at a frequency of ~ 0.4 Hz and found the output signals are quite stable (Fig. S6, Supplementary Information).

7. Demonstration of electrical energy harvesting through prepared shoe insole

As a demonstration of the moldability of the porous composite prepared for possible use in wearable energy harvesting applications, one porous 3D shoe-insole was prepared of thickness 10 mm (thickness/height of base = 3.5 mm and thickness/height of columns = 6.5 mm, Fig. 6d) using the optimal conditions found in earlier experiments (LMA:NaCl:Ecoflex = 3:5:10). Different modes of human motion are

used to generate the output as shown in Fig. 7, whereas Fig. 8a and b shows the corresponding I_{SC} and V_{OC} respectively. It is observed that there is variation of I_{SC} and V_{OC} with different modes of human motion and the I_{SC} and V_{OC} are highest in case of jogging which are ~ 13 μA and ~ 200 V respectively. The different power density obtained in case of various types of human motion (using shoe insole) is given in Fig. S7 (Supplementary Information). The shoe insole produces a maximum instantaneous power of 2.6 mW (instantaneous power density = 13 $\mu\text{W}/\text{cm}^2$) in case of jogging, which can be used to power ECG chips and other small-scale wearable sensors/electronics. The above obtained instantaneous power density is ~ 18 and ~ 32 times higher than previously reported triboelectric foams based on PDMS and CNT/PZT respectively [41,42]. In Fig. 8 (a, b), the same person (73 kg) is used to collect the output (I_{SC} and V_{OC}) of the different types of motion state. In Fig. 8 c, we want to show the effect of a person with a lighter weight on the amount of output current especially in case of jogging. We observed that there is a reduction in the output current (4.15 μA) when the person's weight is less (67 kg). It concluded that larger weight produces larger compression followed by larger output signal as also seen in case of Fig. 4e and f. The frequency of the current (Fig. 8a) and voltage (Fig. 8b) output varies because they are measured separately at different instances. In both cases, a source measurement unit is connected and operated at different modes, i.e. current or voltage sensing mode to obtain the plot shown in Fig. 8 (a, b). Apart from compression, we also presented the output performance of the porous composite based on other kinds of deformation such as stretching, bending and twisting, which are more relevant in case of wearable electronics. To

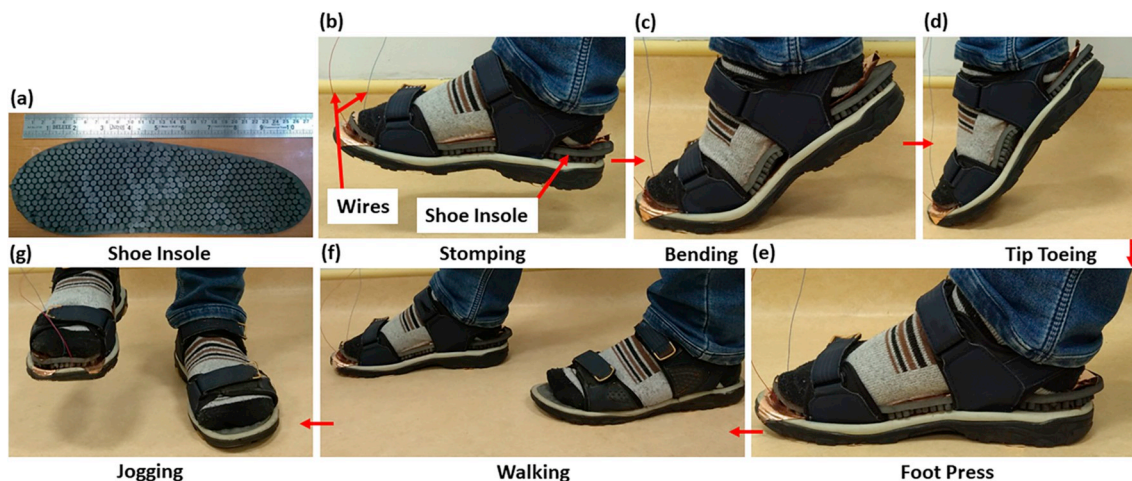


Fig. 7. Demonstration of energy harvesting from human motion using shoe insole prepared from porous LMA-Ecoflex composite [3 wt parts of LMA in Ecoflex matrix (LMA:NaCl:Ecoflex = 3:5:10)]. (a) photograph of a porous LMA-Ecoflex shoe insole used in sandal in between two copper electrodes, (b–g) different stages of human motion and corresponding outputs (I_{SC} , V_{OC}) are given in Fig. 8a and b.

test these deformations, we used a sample of dimension $5\text{ cm} \times 5\text{ cm} \times 0.2\text{ cm}$, coated with conducting carbon grease (MG chemicals, Canada) on both sides as electrodes. The time dependent output current was measured with respect to different % strains (10%–100%), 1.6 cm of bending radii, and 180° twisting. The output charge per cycle was calculated by integrating current over time and presented in Fig. 8d. Stretching and bending was done by a mechanical tester (Multitest 2.5-i), whereas twisting was done manually as given in Fig. S8 (Supplementary Information).

It is observed that there is continuous increase in charge with the increase in % strain (Fig. 8d) and maximum charge per cycle is observed for 100% strain, which is $\sim 88\text{ nC}$. Larger strain compresses the cavities more followed by higher output. Moreover, output energy produced by bending and twisting action are smaller compared to

stretching. The output charge per cycles upon bending and twisting are $\sim 58\text{ nC}$ and $\sim 55\text{ nC}$ respectively. Hence, this type of porous composites can be used as wearable energy harvester to power wearable sensors as it can harvest energy from stretching, bending, and twisting.

8. Porous LMA-Ecoflex composite as force measurement sensor

In this section, we showed the possibility of using the porous composite as a force/weight measurement sensor as a result of capacitance change with different amount of deformations. The effect of loading on the static capacitance of porous composite with the optimal condition (LMA:NaCl:Ecoflex = 3:5:10) and three different sample sizes (thicknesses = 1, 2, 3 cm and area = $5\text{ cm} \times 5\text{ cm}$) is given in Fig. 9a. The variation of displacement with the applied load is given in Fig. 9b.

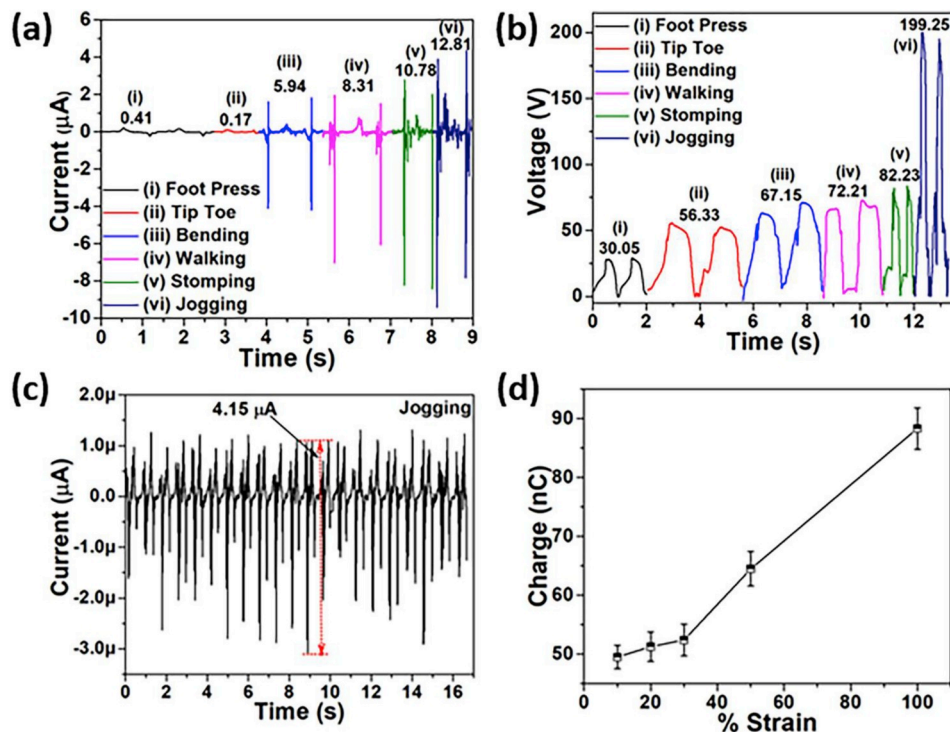


Fig. 8. Output (a) Short circuit current (I_{SC}) and (b) Open circuit voltage (V_{OC}) profile at different stages of human motion: foot pressing, tip-toeing, bending, walking, stomping, and jogging (person's weight = 73 kg), (c) Output short circuit current (I_{SC}) due to jogging of a person of 67 kg weight using shoe insole, and (d) Output charge for composite containing 3 wt parts of LMA in Ecoflex matrix (LMA:NaCl:Ecoflex = 3:5:10) with respect to different % strain [sample dimension = $5\text{ cm} \times 5\text{ cm} \times 0.2\text{ cm}$]. [Maximum percent error $\sim 5\%$].

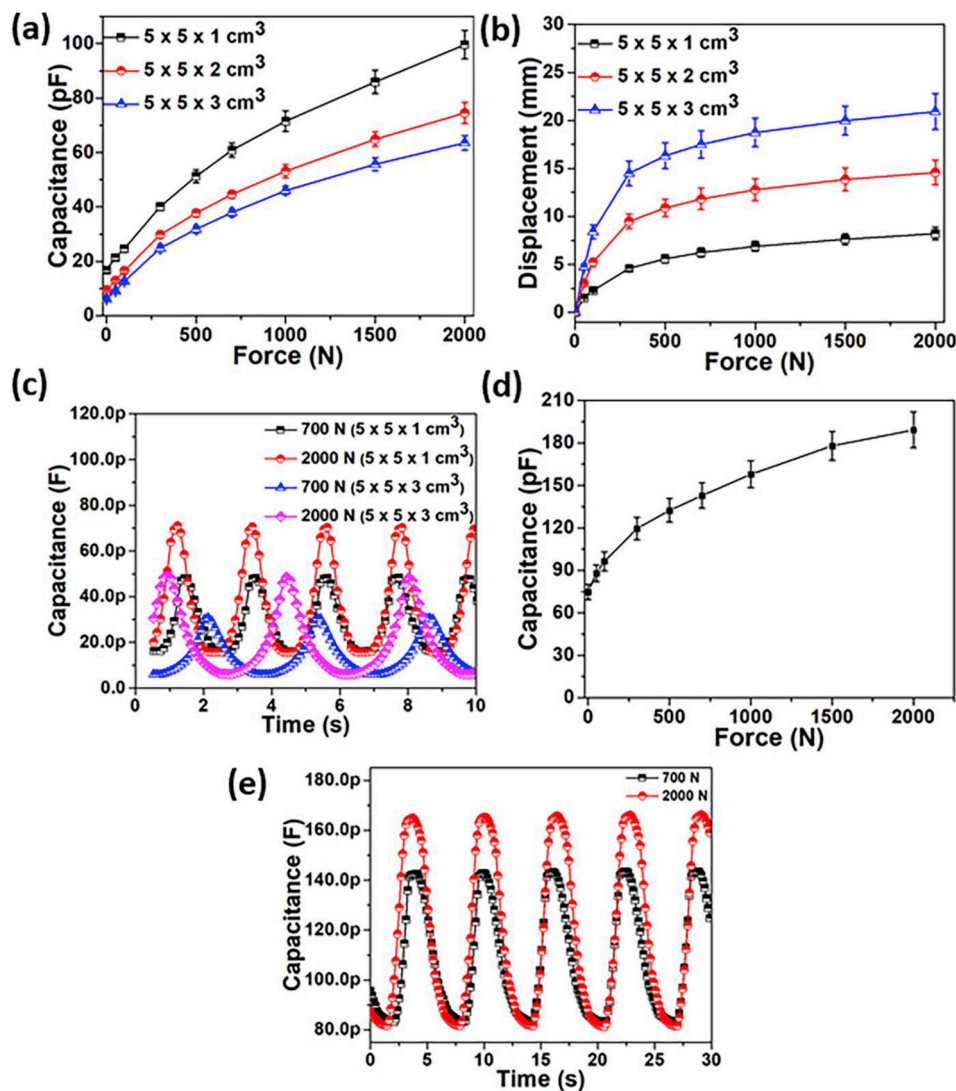


Fig. 9. Variation of (a, b) Capacitance and displacement with applied force respectively for composite with optimum composition and samples of three different thicknesses (1, 2, and 3 cm) and area of $5\text{ cm} \times 5\text{ cm}$ [Maximum percent error $\sim 9\%$], (c) Dynamic capacitance with time at two different cyclic compressive forces (700 N and 2000 N) for samples of two different thicknesses 1 and 3 cm, (d) Variation of static capacitance with applied force, and (e) Variation of dynamic capacitance with time at two different cyclic compressive forces (700 N and 2000 N) on shoe insole [Maximum percent error $\sim 7\%$].

It is observed that there is increase in capacitance/displacement with the increase in applied force. The capacitance of the above samples was also measured under cyclic compressive forces (Fig. 9c). Moreover, we also studied the effect of static/cyclic forces and different forms of human motion (walking, jogging, and jumping) on capacitance of shoe insole and presented in Fig. 9d and e and Fig. 10 respectively. The change in capacitance of the material subjected to different loading conditions allows us to track the weight and force exerted on the legs of a person when it is used as a shoe insole. There are different curve patterns with different forms of human motion (Fig. 10, person's weight = 73 kg), which can give an indication that a person is walking/jogging/jumping. This capacitive sensing requires additional power source when sensing force, assisted by the energy harvested in the triboelectric mode. A possible application could be a physical activity sensor of a person to constantly track the degree of physical activity he/she is undergoing, resulting in a much more accurate fitness monitor.

9. Summary and conclusions

Porous liquid metal alloy-Ecoflex (LMA-Ecoflex) composites have been prepared from Ecoflex elastomer, LMA and NaCl particles, where

NaCl is used as a sacrificial template. These composites have been demonstrated for the first time in TENG application. We found the porous composite prepared with 3 parts of LMA, 5 parts of NaCl in Ecoflex matrix (LMA:NaCl:Ecoflex = 3:5:10), has better performance compared to other composites. The triboelectric foam produced a maximum peak-to-peak short-circuit current (I_{SC}) of $\sim 466\text{ nA}$ (charge density = $\sim 35\text{ }\mu\text{C}/\text{m}^2$) and open circuit voltage (V_{OC}) of $\sim 78\text{ V}$ for a sample of size $5\text{ cm} \times 5\text{ cm} \times 1\text{ cm}$ subjected to 5 mm compression-relaxation cycles, where the output current is $\sim 20\%$ higher than previously reported triboelectric foams based on PDMS and PZT/CNT of equivalent area. The shoe insole produces an instantaneous power of 2.6 mW (power density = $13\text{ }\mu\text{W}/\text{cm}^2$) in case of jogging, which can be used to power ECG chips and other small-scale wearable sensors. The obtained instantaneous power density is found significantly higher than previously reported triboelectric foams based on PDMS and CNT/PZT. We also found that there is change in capacitance with loading of different static or cyclic forces. So, this type of composites can be used as weight/force measurement sensor. These porous composites can also be used as wearable energy harvester to power wearable sensors as it can harvest energy from stretching, bending, and twisting.

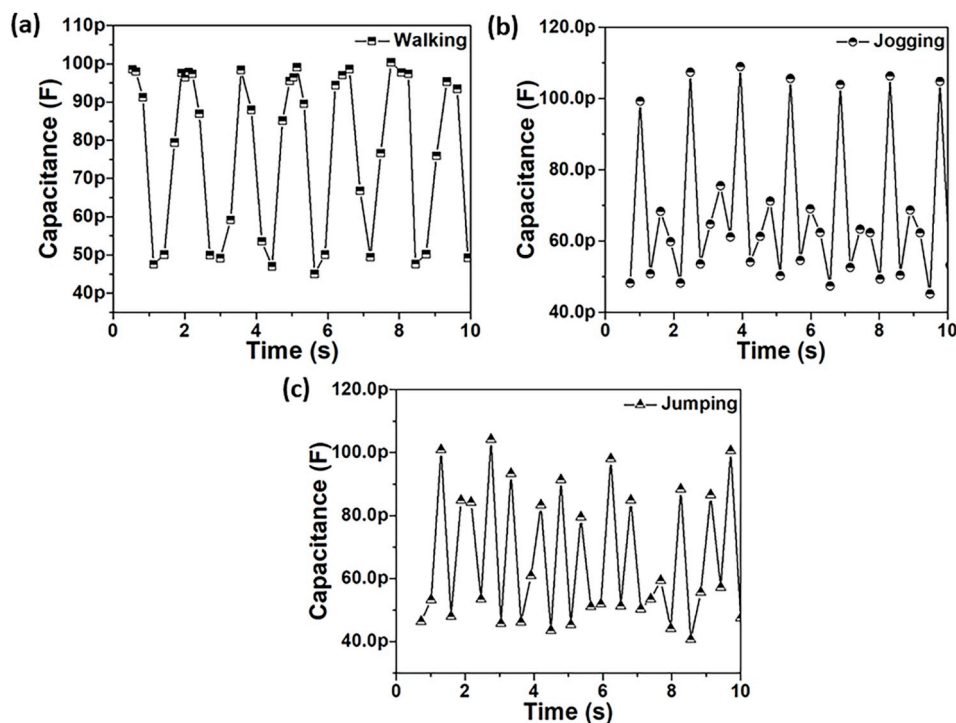


Fig. 10. Variation of capacitance with different forms of human motion (walking, jogging, and jumping).

Conflicts of interest

There are no conflicts to declare.

Acknowledgement

The authors would like to thank Handiyadi Tantiono for helping us to take microscope images using their Keyence microscope (VHX 5000). Authors are thankful to Li Yang and Fangfang (Bruker, Singapore) for EFM measurement.

The work was funded by Singapore National Research Foundation's Returning Singapore Scientist Scheme (Grant Ref: NRF-RSS2015-003), Hybrid Integrated Flexible Electronic Systems (HiFES) Program (hifes.nus.edu.sg), E6Nanofab at National University of Singapore (NUS).

Appendix A. Supplementary data

Supplementary data to this article can be found online at <https://doi.org/10.1016/j.nanoen.2019.103912>.

References

- [1] A.D. Valentine, T.A. Busbee, J.W. Boley, J.R. Raney, A. Chortos, A. Kotikian, J.D. Berrigan, M.F. Durstock, J.A. Lewis, *Adv. Mater.* 29 (1) (2017) 1703817.
- [2] M.D. Dickey, *Adv. Mater.* 29 (1) (2017) 1606425.
- [3] S.W. Jin, J. Park, S.Y. Hong, H. Park, Y.R. Jeong, J. Park, S.S. Lee, J.S. Ha, *Sci. Rep.* 5 (1) (2015) 11695.
- [4] X. Pu, L. Li, H. Song, C. Du, Z. Zhao, C. Jiang, G. Cao, W. Hu, Z.L. Wang, *Adv. Mater.* 27 (2015) 2472.
- [5] X. Pu, M. Liu, X. Chen, J. Sun, C. Du, Y. Zhang, J. Zhai, W. Hu, Z.L. Wang, *Science Advances* 3 (5) (2017) e1700015(1).
- [6] A. Chortos, J. Liu, Z. Bao, *Nat. Mater.* 15 (2016) 937.
- [7] S. Taccola, F. Greco, E. Sinibaldi, A. Mondini, B. Mazzolai, V. Mattoli, *Adv. Mater.* 27 (2015) 1668.
- [8] S. Park, K. Mondal, R.M. Treadway 3rd, V. Kumar, S. Ma, J.D. Holbery, M.D. Dickey, *ACS Appl. Mater. Interfaces* 10 (2018) 11261.
- [9] M.D. Bartlett, E.J. Markvicka, C. Majidi, *Adv. Funct. Mater.* 26 (2016) 8496.
- [10] J. Byun, B. Lee, E. Oh, H. Kim, S. Kim, S. Lee, Y. Hong, *Sci. Rep.* 7 (1) (2017) 45328.
- [11] X. Pu, M. Liu, X. Chen, J. Sun, C. Du, Y. Zhang, J. Zhai, W. Hu, Z.L. Wang, *Science Advances* 3 (5) (2017) e1700015(1).
- [12] X. Wang, Y. Yin, F. Yi, K. Dai, S. Niu, Y. Han, Y. Zhang, Z. You, *Nano Energy* 39 (2017) 429.
- [13] J. Sun, X. Pu, M. Liu, A. Yu, C. Du, J. Zhai, W. Hu, Z.L. Wang, *ACS Nano* 12 (6) (2018) 6147–6155.
- [14] S. Nayak, T.K. Chaki, D. Khastgir, *Ind. Eng. Chem. Res.* 53 (2014) 14982.
- [15] Z.L. Wang, J. Chen, L. Lin, *Energy Environ. Sci.* 8 (2015) 2250.
- [16] J. Wang, S. Li, F. Yi, Y. Zi, J. Lin, X. Wang, Y. Xu, Z.L. Wang, *Nat. Commun.* 7 (1) (2016) 12744.
- [17] X. Chen, Y. Wu, J. Shao, T. Jiang, A. Yu, L. Xu, Z.L. Wang, *Small* 13 (1) (2017) 1702929.
- [18] L. Dhakar, P. Pitchappa, F.E.H. Tay, C. Lee, *Nano Energy* 19 (2016) 532.
- [19] Q. Shi, H. Wang, T. Wang, C. Lee, *Nano Energy* 30 (2016) 450.
- [20] R.K. Gupta, Q. Shi, L. Dhakar, T. Wang, C.H. Heng, C. Lee, *Sci. Rep.* 7 (1) (2017) 41396.
- [21] H. Wang, H. Wu, D. Hasan, T. He, Q. Shi, C. Lee, *ACS Nano* 11 (10) (2017) 10337.
- [22] H. Zhang, Y. Yang, X. Zhong, Y. Su, Y. Zhou, C. Hu, Z.L. Wang, *ACS Nano* 8 (2014) 680.
- [23] S. Wang, X. Mu, X. Wang, A.Y. Gu, Z.L. Wang, Y. Yang, *ACS Nano* 9 (2015) 9554.
- [24] S. Wang, X. Wang, Z.L. Wang, Y. Yang, *ACS Nano* 10 (2016) 5696.
- [25] S. Lee, Y. Lee, D. Kim, Y. Yang, L. Lin, Z.-H. Lin, W. Hwang, Z.L. Wang, *Nano Energy* 2 (2013) 1113.
- [26] Y. Wu, X. Zhong, X. Wang, Y. Yang, Z.L. Wang, *Nano Research* 7 (2014) 1631.
- [27] Y. Yang, Z.L. Wang, *Nano Energy* 14 (2015) 245.
- [28] Y. Su, Y. Yang, X. Zhong, H. Zhang, Z. Wu, Y. Jiang, Z.L. Wang, *ACS Appl. Mater. Interfaces* 6 (2014) 553.
- [29] X. Wen, Y. Su, Y. Yang, H. Zhang, Z.L. Wang, *Nano Energy* 4 (2014) 150.
- [30] Y. Wu, X. Wang, Y. Yang, Z.L. Wang, *Nano Energy* 11 (2015) 162.
- [31] J. Chun, J.W. Kim, W-s Jung, C.-Y. Kang, S.-W. Kim, Z.L. Wang, J.M. Baik, *Energy Environ. Sci.* 8 (2015) 3006.
- [32] J. Chen, H. Guo, X. He, G. Liu, Y. Xi, H. Shi, C. Hu, *ACS Appl. Mater. Interfaces* 8 (2016) 736.
- [33] D. Kim, S.-J. Park, S.-B. Jeon, M.-L. Seol, Y.-K. Choi, *Advanced Electronic Materials* 2 (2016) 1500331.
- [34] X. Xia, J. Chen, H. Guo, G. Liu, D. Wei, Y. Xi, X. Wang, C. Hu, *Nano Research* 10 (2017) 320.
- [35] G. Cai, J. Wang, K. Qian, J. Chen, S. Li, P.S. Lee, *Advanced Science* 4 (1) (2017) 1600190.
- [36] Z.L. Wang, *Faraday Discuss* 176 (2014) 447.
- [37] Z.L. Wang, *ACS Nano* 7 (2013) 9533.
- [38] Y. Zi, S. Niu, J. Wang, Z. Wen, W. Tang, Z.L. Wang, *Nat. Commun.* 6 (1) (2015) 8376.
- [39] S.H. Jeong, S. Chen, J. Huo, E.K. Gamstedt, J. Liu, S.L. Zhang, Z.B. Zhang, K. Hjort, Z. Wu, *Sci. Rep.* 5 (1) (2015) 18257.
- [40] J. Wang, C. Wu, Y. Dai, Z. Zhao, A. Wang, T. Zhang, Z.L. Wang, *Nat. Commun.* 8 (1) (2017) 88.
- [41] Y.J. Fan, X.S. Meng, H.Y. Li, S.Y. Kuang, L. Zhang, Y. Wu, Z.L. Wang, G. Zhu, *Adv. Mater.* 29 (1) (2017) 1603115.
- [42] S.W. Ma, Y.J. Fan, H.Y. Li, L. Su, Z.L. Wang, G. Zhu, *ACS Appl. Mater. Interfaces* 10 (2018) 33105.
- [43] H. Chen, L. Miao, Z. Su, Y. Song, M. Han, X. Chen, X. Cheng, D. Chen, H. Zhang,

- Nano Energy 40 (2017) 65.
- [44] T. Majid, M. Virgilio, B. Lucia, M. Barbara, Triboelectric composite for mechanical energy harvesting and sensing, (2017), p. 1 US 9 , 748 , 868 B2. US.
- [45] H.Y. Mi, X. Jing, Z. Cai, Y. Liu, L.S. Turng, S. Gong, Nanoscale 10 (2018) 23131.
- [46] P. Cheolmin, P. Chanho, S. Giyoung, C. Sun Man, Nano-porous Thin Film, Methods of Fabricating Thereof and Triboelectric Generator Using the Same, (2018) US 2018/0294745 A1. US.
- [47] Y. Li, S. Nayak, Y. Luo, Y. Liu, H.K. Salila Vijayalal Mohan, J. Pan, Z. Liu, C.H. Heng, A.V. Thean, Materials 12 (2019) 1458.
- [48] Y. Li, Y. Luo, S. Nayak, Z. Liu, O. Chichvarina, E. Zamburg, X. Zhang, Y. Liu, C.H. Heng, A.V.-Y. Thean, Advanced Electronic Materials 5 (2) (2018) 1800463 (1).
- [49] Z. Lin, Z. Wu, B. Zhang, Y.-C. Wang, H. Guo, G. Liu, C. Chen, Y. Chen, J. Yang, Z.L. Wang, Advanced Materials Technologies 4 (2019) 1800360.
- [50] T.-C. Hou, Y. Yang, H. Zhang, J. Chen, L.-J. Chen, Z. Lin Wang, Nano Energy 2 (2013) 856.
- [51] G. Zhu, P. Bai, J. Chen, Z. Lin Wang, Nano Energy 2 (2013) 688.
- [52] C. Yang, Y. Lin, C.W. Nan, Carbon 47 (2009) 1096.
- [53] U.O. Uyor, A.P. Popoola, O. Popoola, V.S. Aigbodion, Adv. Polym. Technol. 37 (8) (2018) 2838.
- [54] J. Chen, X. Wang, X. Yu, L. Yao, Z. Duan, Y. Fan, Y. Jiang, Y. Zhou, Z. Pan, J. Mater. Chem. C 6 (2018) 271.



Devendra Singh (Ph.D., IIT Bombay, India, 2015) is Research Fellow in the Department of Electrical & Computer Engineering at NUS, Singapore. He worked for three years as a postdoctoral fellow in KAUST-KSA at Department of Electrical as well as Mechanical Engineering (KAUST & Boeing funded project). Prior to his graduation, he did Master's in Advanced Materials Science & Technology (M.Tech.) with a gold medal from NIT Durgapur, and Master's in Physics (M.Sc.) from Kanpur University, India. His research interests include the fabrication and characterization of advanced oxide-based semiconductor devices for flexible electronics, optoelectronics and energy harvesting applications.



Chengkuo Lee received his Ph.D. degree in Precision engineering from The University of Tokyo in 1996. Currently, he is the director of Center for Intelligent Sensors and MEMS, and an Associate Professor in the Department of Electrical and Computer Engineering, National University of Singapore, Singapore. In 2001, he cofounded Asia Pacific Microsystems, Inc., where he was the Vice President. From 2006 to 2009, he was a Senior Member of the Technical Staff at the Institute of Microelectronics, A-STAR, Singapore. He has contributed to more than 300 international conference papers and extended abstracts and 300 peer-reviewed international journal articles.



Soo Jin Adrian Koh is an Assistant Professor at the Department of Mechanical Engineering, National University of Singapore (NUS). He received his PhD in Integrative Sciences & Engineering at NUS in 2008. He was a Post-Doctoral Fellow at the Harvard School of Engineering & Applied Sciences between 2008 and 2010. His research interests are motion-based energy harvesting, soft robotics actuation and autonomous sensing of civil structures. He is an invited speaker, workshop lecturer and keynote speaker to notable conferences like the SPIE EAPAD, MRS Fall, ASME/IEEE and EuroEAP.



Patrick's (Associate Professor, NUS) research centered around making new connection found in new emergence between art, design, technology, business, psychology and sociology. His works often explored the evolving relationship between human, society and technology. Works and projects he has created or directed have been represented by or exhibited in galleries and museums around the world, including Triennale de Milano and MoMA in New York. He sits on the jury of numerous award panels including the Red Dot Design Award, Dyson Design Award and the Jury Chair for the President's Design Award. In 2013, he received the President's Designer of the Year Award.



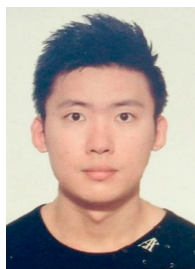
Aaron Voon-Yew Thean is the Director of HiFES and a Professor of Electrical and Computer Engineering at the National University of Singapore. He also serves as the Co-Director for A*Star SIMTech – NUS Joint laboratory for Large-Area Flexible Hybrid Electronics. He has previously served as IMEC's Vice President of Logic Technologies where he led a research consortium on advanced semiconductor technologies. He was awarded the 2001 Gregory Stillman Semiconductor Research Award for his PhD work. He has published over 300 technical papers and holds more than 50 U.S. patents for inventions in the field of advanced electronics.



Suryakanta Nayak received his PhD degree in "Smart Polymer-ceramic Nanocomposites" from IIT Kharagpur, India in 2015. Currently, he is working as a postdoctoral research fellow in Prof. Aaron Thean's research group at National University of Singapore (NUS). Prior to joining Aaron Thean's research group, he worked with Dr. S.J.A. Koh, NUS. Prior to PhD, he has two years of industrial research experience from R & D, Tata Steel Limited, Jamshedpur, India. His research interests are soft composite materials, motion-based energy harvesting, and different type of sensors. He is in editorial board of two international journals. Personal Web Page: <https://suryakantanayak.weebly.com/>



Yida Li graduated from the National University of Singapore with a B. Eng (1st Hons) and Ph.D. in Integrative Science and Engineering Program. He is currently a research fellow in National University of Singapore working under Professor Aaron Thean. He has previously served in TSMC, Hsinchu working on metal deposition and silicidation process at 7 nm technology node and beyond. With Professor Thean, he is now working on next generation neuromorphic computing devices using metal-oxides/novel 2D materials, as well as additive processing and heterogeneous integration of materials to create the new generation of hybrid flexible/wearable electronics and biomedical devices.



Willie Tay is a senior designer at Design Incubation Centre, Division of Industrial Design, School of Design and Environment, National University of Singapore.



Evgeny Zamburg is a Research Fellow at National University of Singapore. He received PhD in nanoelectronics from Southern Federal University, Russia. He deals with the development fabrication process of devices and structures for nanoelectronics. He has worked as a researcher within various fellowship programs in Swiss Federal Institute of Technology in Lausanne (Switzerland), National Chiao Tung University (Taiwan), IBM Research – Zurich (Switzerland), and Technical University of Munich (Germany). He has been a winner of numerous awards for outstanding young investigators from: IBM Research, Nokia, Swiss Government, German Academic Exchange Service, Russian Academy of Sciences, the Russian President, etc.